BACHELOR THESIS

BOUNDED PROPULSION OF HELICAL DEVICE WITH NEAR-ZERO ANGLE OF ATTACK

ILSE A.A. EKKELKAMP

FOR BACHELOR BIOMEDICAL TECHNOLOGY

DEPARTMENT - FACULTY

BIOMECHANICAL ENGINEERING – ENGINEERING TECHNOLOGY

EXAMINATION COMMITTEE

Dr. Islam Khalil

Prof. Dr. Sarthak Misra

Dr. Ir. Arvid Keemink

DOCUMENT NUMBER

BE-945

DATE

15-09-2023

UNIVERSITY OF TWENTE.

SURGICAL ROBOTICS LABORATORY

UNIVERSITY OF TWENTE.

FACULTY OF ENGINEERING TECHNOLOGY
DEPARTMENT OF BIOMECHANICAL ENGINEERING

Declaration of consent

By means of this declaration of consent I, Ilse Ehlenkamp 2258455 (name student and student number), give permission to the University of Twente, located at Drienerlolaan 5, 7522 NB in Enschede, to use work from my bachelor assignment (course name), including my name (from here on together referred to as 'work'), under the conditions as described below:

1. I give permission to use my work *for educational purposes during the* course or module: bachelor assignment
   for study program(s): biomedical technology
   I give permission to use:
   - (●) All my work from the specified course (pictures, drawings, prototypes, report, code, etc.)
   - ( ) All of my work, except the following: _____
   - ( ) None of my work

2. I give permission to use my work for future analysis, modification and (scientific) publication
   - (●) All my work from the specified course (pictures, drawings, prototypes, report, code, etc.)
   - ( ) All of my work, except the following: _____
   - ( ) None of my work

For reuse of my work I will always receive proper attribution according to academic and/or licensing standards and in compliance with the Copyright Act and/or will receive (co)authorship of manuscripts according to academic standards.

My permission only applies to the specific data, institution and study program(s) described above. The university needs to request my permission again to reuse my work for any purpose not covered in the agreement stated above. I can withdraw my consent at any time. I am aware that some copies of my work may be made and used exclusively for own exercise, study or use of the person who makes the copies or gives the assignment to make the copies exclusively for his/her own use (article 16 b (1) Copyright Act).

Name student + student number	Name of supervisor + employee number
Ilse Ehlenkamp S2258455	Islam S. M. Khalil
Date	**Date**
17/11/2022	18/11/2022
Student's signature	**Supervisor's signature**
	Islam Khalil

CONTENTS

Bounded propulsion of helical device with near-zero angle of attack

Ilse A. A. Ekkelkamp

***Abstract*— Untethered helical magnetic devices (UHMDs) seem promising in the world of minimally invasive medicine in hard-to-reach areas of the body. Moving the helical devices with a small angle of attack (AoA) could prove useful when the device swims in a lumen-like environment or environments with heterogeneous structural properties. Moreover, using open-loop control can prove useful when using imaging techniques with a low resolution to map the location and orientation of the device. It was shown which physical boundaries are needed to achieve bounded runs of the UHMD with a small AoA. When swimming with a small AoA, there is an equilibrium between the gravitational force and the magnetic pulling force, causing the UHMD to propel with active suspension. A numerical model based on resistive force theory (RFT) was used to predict the input values of the actuator and a reduced order model was used to predict the behaviour of the UHMD as a result of the rotation of the RPM, which were both validated experimentally. In the experiments, it was shown it is possible to create a bounded response of the UHMD by either gravity compensation or active suspension. Though one real bounded case was recorded with propulsion with a small AoA, the system is still lacking robustness due to factors like wobbling and drift.**

I. INTRODUCTION

A type of magnetic microrobots, untethered helical magnetic devices (UHMDs), seems promising for minimally invasive medicine. The device could possibly be used for multiple applications in hard-to-reach areas in the body when actuated by an externally applied magnetic field [1], [2], [3]. From targeted therapy, like targeted drug delivery [4] and removing material by mechanical means [5], to steering controllable structures [2], [6] and sensing of physical signals [7]. The actuation of the device is done by using a rotating permanent magnet (RPM), which spins at a certain frequency and moves along a trajectory, causing the UHMD to rotate as well and to trail behind the magnetic field about the long axis. The propulsion of the device is achieved by the helical shape of the tail, which creates a thrust when the body of the device rotates. This type of propulsion is suitable for a low-Reynolds number regime [8].

Mahoney et al. achieved control of a UHMD by actuating their device under a certain large angle of attack, thus using the thrust created by the device to counteract gravity. By controlling the actuator, they moved the device as desired [9]. However, UHMDs are likely to be deployed in lumen-like environments such as arteries (with a diameter of 4 mm) or the spinal cord (which holds channels with a diameter as small as 1.5 mm), or to navigate through larger volumes such as the bladder to reach the kidneys [2] (Fig. 2(A)). These lumens vary in length for the different organs, from the ureter (250 mm) to the cerebral aqueduct in the brain (11.8 mm). The UHMDs will also encounter environments

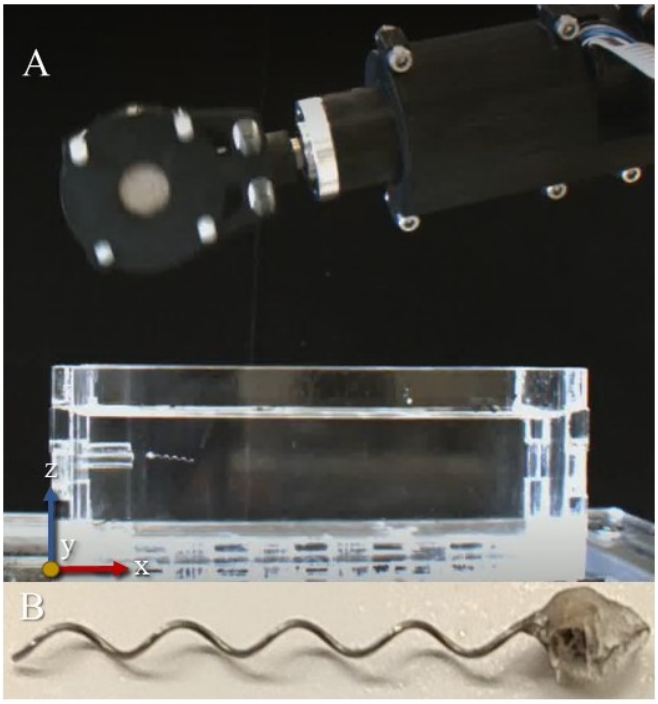

Fig. 1. (A) An RPM is connected to a robotic manipulator. The magnetic field produced by the RPM actuates the untethered helical magnetic device (UHMD) which creates a thrust, enabling it to swim along the $\mathbf{x}$-axis. (B) The UHMD consists of a small, cylindrical magnet attached to an aluminium wire wound in a helical shape to create the tail with a length of 11.7 mm.

with heterogeneous structural properties, like the interface between two mediums or the changing quantity of cells and molecules in bodily fluids [10]. Take for example the application of entering the kidneys to treat kidney stones [2] (Fig. 2 (A)), drilling through soft tissues to the center of a tumor to deliver treatment [11] or drilling through a blood clot [12]. Such an interface is likely to require the microrobot to swim along a straight trajectory toward the target [12] (Fig. 2. Behaving in a lumen requires a horizontal orientation, thus a small angle of attack (AoA), due to the natural confinements of the environment.

To enforce gravity compensation of the helical robot, a closed-loop system can be used to measure and control the device [13], but it is shown that detecting the AoA using techniques like ultrasound or x-ray is still challenging (Fig. 2(C)) [14], [15], [16]. Being able to control the device using open-loop would eliminate the need for very precise imaging.

When controlling helical robots, it is important to take the frequency at which the device is actuated into account. The forward velocity increases linearly with the frequency

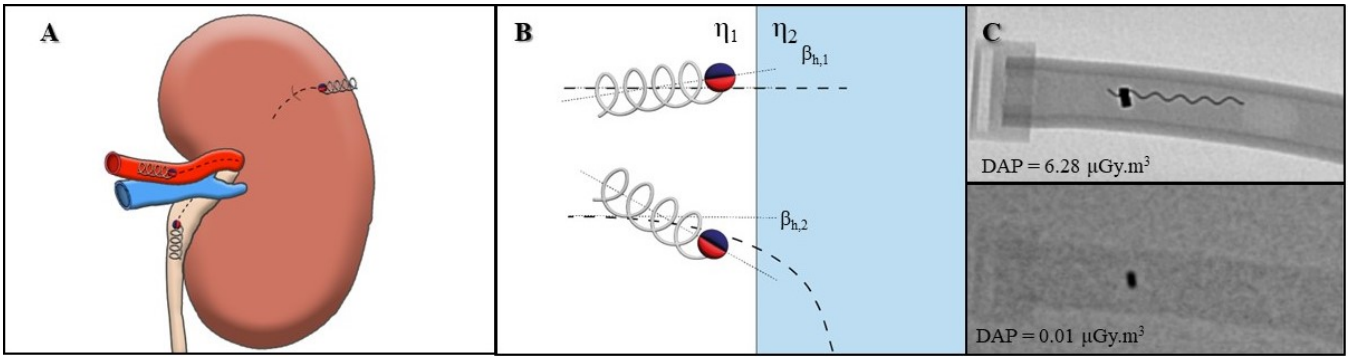

Fig. 2. Different scenarios in which swimming with a small angle of attack (AoA) is more convenient. (A) Propulsion through a lumen would require a small AoA to remain inside the natural boundaries. For example, when accessing the kidney by the renal artery or the ureter. It also shows a case of accessing the kidney from the outside, drilling its way into the organ. (B) When passing through environments with heterogeneous structural properties, a small AoA is required for the device to keep the same trajectory [12]. The viscosity η of the mediums differs, causing a different response of the UHMD at the interface, depending on the AoA. (C) Imaging techniques can be used to determine the device's orientation for controlling the trajectory. However, when the resolution is too low, the orientation can no longer be determined [18]. Opting for open-loop control with active suspension of the device would eliminate the need to know the orientation.

until a 'step-out' frequency is reached. Beyond this point, the device can no longer stay in sync with the rotation speed of the RPM, resulting in a drastic decrease in forward velocity [1].

In this paper, the input-output boundedness of a magnetically actuated helical device in a low Reynolds number regime is experimentally investigated by varying the inputs (rotational frequency, distance between the RPM and UHMD, translational velocity and pitch angle) of the actuator, a rotating permanent magnet. The different inputs are based on a resistive force theory (RFT) model earlier investigated and validated [17] and an alternative method of predicting the position of the UHMD using a reduced order model [18] is also examined.

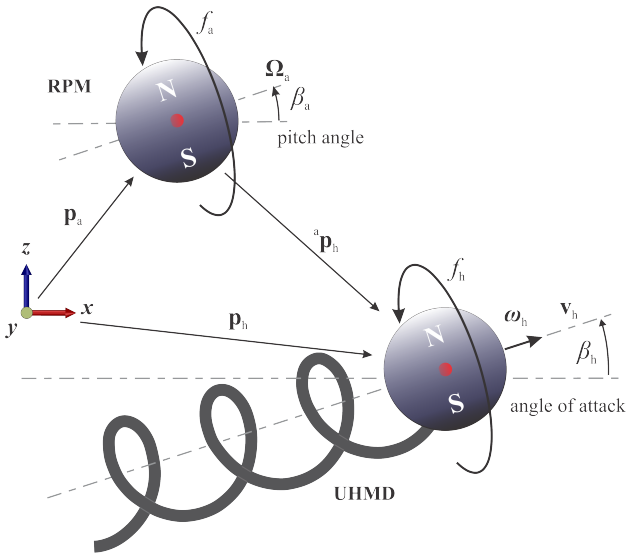

Fig. 3. A UHMD is actuated by an RPM, such that the rotation of the device causes a thrust which propels the device. The position of the UHMD with respect to the device is denoted by ${}^{\mathrm{a}}\mathbf{p}_{\mathrm{h}}$ and the angle of attack (AoA) by β_{h}. The UHMD spins at frequency f_{h}, which is in sync with the frequency f_{a} of the RPM [17].

II. BOUNDED BEHAVIOR OF THE OPEN-LOOP CONTROLLED UHMD

When actuating the UHMD with an RPM, the different input parameters of the RPM influence the trajectory of the helical device. When set correctly, the pulling force of the magnet and gravitational forces are self-compensated and the helical device follows a straight path with a small AoA. To show how to find the different parameters, a 6-DOF model was made in earlier work [17] on basis of resistive force theory (RFT) in which the device swims with active suspension.

A. Helical Propulsion in Low-Reynolds Number Regime

The RPM generates a magnetic field $\mathbf{B}({}^{\mathrm{a}}\mathbf{p}_{\mathrm{h}})$ and spins with a frequency f_{a} at a pitch angle $\beta_{\mathbf{a}}$, which controls the rotation axis $\widehat{\mathbf{\Omega}}_{\mathrm{a}} \in \mathbb{R}^{3\times 1}$ (The symbol $\widehat{\ }$ denotes unit-length vector) with respect to the $\mathbf{x}$-axis (Fig. 3). We consider a UHMD with a tail length of l and a magnetic moment $\mathbf{m}_{\mathrm{h}}$. The position of the UHMD at any moment in time is given by ${}^{\mathrm{a}}\mathbf{p}_{\mathrm{h}} = [{}^{\mathrm{a}}p_{\mathrm{h}_x}, {}^{\mathrm{a}}p_{\mathrm{h}_y}, {}^{\mathrm{a}}p_{\mathrm{h}_z}]^T$, with respect to the frame of reference $\{\boldsymbol{x}, \boldsymbol{y}, \boldsymbol{z}\}$. The UHMD is magnetically actuated at position ${}^{\mathrm{a}}\mathbf{p}_{\mathrm{h}}$, after which a magnetic force and magnetic torque will be produced on the UHMD:

$$\begin{pmatrix} \mathbf{f}_{\mathrm{m}} \\ \tau_{\mathrm{m}} \end{pmatrix} = \begin{pmatrix} (\mathbf{m}_{\mathrm{h}} \cdot \nabla)\mathbf{B}({}^{\mathrm{a}}\mathbf{p}_{\mathrm{h}}) \\ \mathbf{m}_{\mathrm{h}} \times \mathbf{B}({}^{\mathrm{a}}\mathbf{p}_{\mathrm{h}}) \end{pmatrix}. \tag{1}$$

The magnetic field of the RPM causes the UHMD to rotate with a frequency f_{h} at an angle of attack β_{h} with respect to the $\mathbf{x}$-axis. This rotation causes a translational velocity of the UHMD $\mathbf{v}_{\mathrm{h}} \in \mathbb{R}^{3\times 1}$. The RPM moves along the positive $\mathbf{x}$-axis with respect to the UHMD, to reduce the change in the position vector ${}^{\mathrm{a}}\mathbf{p}_{\mathrm{h}}$ and to ensure the control of motion of the device along the set trajectory of the RPM. Since the device swims in the low Reynolds number regime, the internal forces of the device can be neglected. The response of the UHMD to the RPM is given by the following balance between forces and torques, which is influenced by the

magnetic pulling forces, the viscosity of the fluid creating a drag forces and gravitational forces:

$$\begin{pmatrix} \mathbf{f}_{\mathrm{m}} + \mathbf{f}_{\mathrm{visc}} + \mathbf{f}_{\mathrm{g}} \\ \boldsymbol{\tau}_{\mathrm{m}} + \boldsymbol{\tau}_{\mathrm{visc}} + \boldsymbol{\tau}_{\mathrm{g}} \end{pmatrix} = \mathbf{0}. \tag{2}$$

Here, $\mathbf{f}_{\mathrm{visc}}$ and $\mathbf{f}_{\mathrm{g}}$ are the drag force and force due to gravity, respectively, and $\boldsymbol{\tau}_{\mathrm{visc}}$ and $\boldsymbol{\tau}_{\mathrm{g}}$ are their corresponding torques. The drag forces and torques can be determined using the equation below:

$$\begin{pmatrix} \mathbf{f}_{\mathrm{visc}} \\ \boldsymbol{\tau}_{\mathrm{visc}} \end{pmatrix} = -\left(\int_0^{l_1} \mathcal{M}\, \mathrm{d}s + \begin{bmatrix} \mathcal{A} & \mathcal{B} \\ \mathcal{B}^T & \mathcal{D} \end{bmatrix} \right) \begin{pmatrix} \mathbf{v}_{\mathrm{h}} \\ \boldsymbol{\omega}_{\mathrm{h}} \end{pmatrix}, \tag{3}$$

where $\mathcal{M} \in \mathbb{R}^{6\times6}$ is the resistance of the helix and is integrated over the length of the tail l, $\mathcal{A} \in \mathbb{R}^{3\times3}$, $\mathcal{B} \in \mathbb{R}^{3\times3}$, and $\mathcal{D} \in \mathbb{R}^{3\times3}$ are the sub-matrices of the head's resistance. These are multiplied with the linear swimming velocity $\mathbf{v}_{\mathrm{h}}$ and the angular velocity ω_{h}. The gravitational forces and torques are found by:

$$\begin{pmatrix} \mathbf{f}_{\mathrm{g}} \\ \boldsymbol{\tau}_{\mathrm{g}} \end{pmatrix} = \begin{pmatrix} V(\rho_{\mathrm{d}} - \rho_{\mathrm{f}})\; g\; \mathbf{R} \\ (\mathbf{r}_{\mathrm{CoV}} - \mathbf{r}_{\mathrm{CoM}}) \times \mathbf{f}_{\mathrm{g}} \end{pmatrix}. \tag{4}$$

where the gravitational force is calculated using the relative mass of the UHMD in the surrounding fluid, determined by the volume of the device V and the difference between device density (ρ_{d}) and fluid density (ρ_{f}), and the gravitational constant g. The gravitational torque is given by the distance $\mathbf{r}$ of the centre of mass (CoM) and centre of volume (CoV) of the device, cross product with the gravitational force. The rotation matrix $\mathbf{R} \in \mathbb{R}^{3\times3}$ is added due to the rotation of the UHMD will undergo due to gravity.

B. Input-Output Gain

To investigate the input-output boundedness, the input-output gain is determined by solving Equation (1) and (2):

$$\gamma := \frac{y}{u} := \frac{\min({}^{\mathrm{a}}\mathbf{p}_{\mathrm{h}_z}(t)) - \max({}^{\mathrm{a}}\mathbf{p}_{\mathrm{h}_z}(t))}{{}^{\mathrm{a}}\mathbf{p}_{\mathrm{h}_z}(t_0)}. \tag{5}$$

By solving the force and torque balance in Equation (2), the gain can be determined and thus the input-output boundedness. For a bounded case, as $t \to \infty$, it is required that $\gamma < 1$. If $\gamma > 1$, it signifies that the device has travelled more along the $\mathbf{z}$-axis than the initial distance between the RPM and UHMD. The lower the value of γ, the more the device stayed in a straight line along the $\mathbf{z}$-axis.

C. Previous results numerical model

In previous work [17], the gain was calculated for different representative cases with varying inputs. To calculate the gain, ${}^{\mathrm{a}}\mathbf{p}_{\mathrm{h}}(t)$ must be determined for all time. By moving the RPM in a circular trajectory, this was achieved in the easiest way. The results of the model showed that a bounded case was achieved for $|{}^{\mathrm{a}}\mathbf{p}_{\mathrm{h}}(t_0)| = 150$ mm, $\beta_{\mathrm{a}} = 12.7°$, $f_{\mathrm{a}} = 3.3$ Hz, and $\dot{\gamma}_{\mathrm{a}} = 1.8°$/s (velocity along a circular path). The gain for this case was $\gamma = 0.252$, where the device remained bounded for all future time.

When simulating straight runs, different values are found for the input parameters when compared to the values found for a circular trajectory. Fig. 4 shows a bounded case for 400 s with a gain of $\gamma = 0.069$, in which the helical device follows a straight line along the $\mathbf{x}$-axis and has a drift along the $\mathbf{y}$-axis. The RPM is set to move with the drift of the device, such that $\mathbf{p}_{\mathrm{a}} = [p_x, p_y, 0]^T$. For this case, the found values were $|{}^{\mathrm{a}}\mathbf{p}_{\mathrm{h}}(t_0)| = 140$ mm, $\beta_{\mathrm{a}} = 12.7°$, $f_{\mathrm{a}} = 3.3$ Hz, $\mathbf{v}_{\mathrm{a,x}} = 1.8$ mm/s and $\mathbf{v}_{\mathrm{a,y}} = 0.5$ mm/s. The model shows that without moving the RPM with the drift, the UHMD will drift out of the influence of the magnetic field, causing it to fall due to the pull of gravity. It also shows that achieving a bounded case for a long period of time proves difficult because small changes in the parameters cause the $\mathbf{z}-$position of the device to become unbounded.

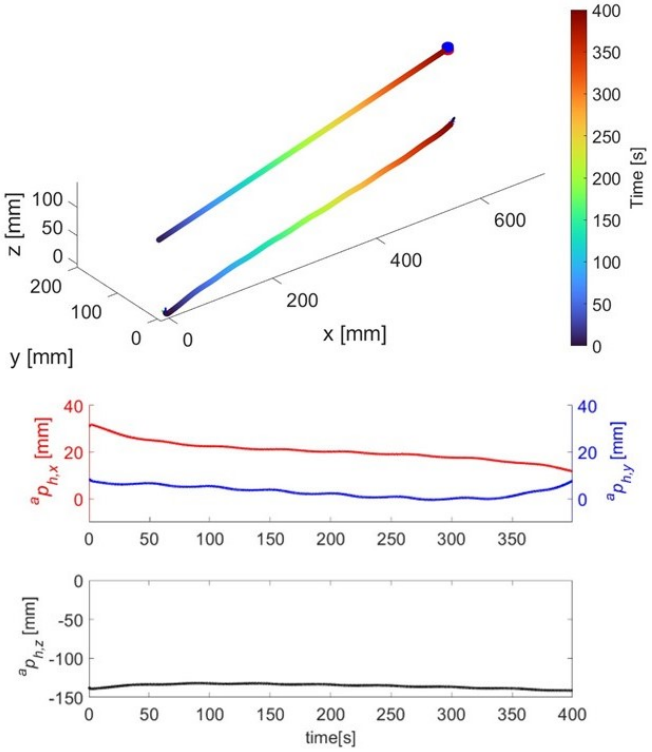

Fig. 4. The model shows a bounded scenario where the UHMD follows a straight line along the $\mathbf{x}$-axis for 400 s, but also drifts along the $\mathbf{y}$-axis. The RPM, shown as the blue/red cilinder, follows a straight trajectory such that $\mathbf{p}_{\mathrm{a}} = [p_x, p_y, 0]^T$. The pitch angle of the RPM was $\beta_{\mathrm{a}} = 12.7°$ and the gain for the bounded section $\gamma = 0.069$.

D. Reduced Order Model

Another method can be used to determine the position of the UHMD with respect to the RPM ${}^{\mathrm{a}}p_{\mathrm{h}_z}$, for which the solving of Equation (2) is not needed. When regarding the UHMD with a small AoA, we can assume that the viscous force acting on the helical body is the same as the viscous force acting on a straight filament of the same length, l_1. We also assume that the RPM and UHMD rotate in synchrony, as long as actuated below step-out. In this case, the velocity of the UHMD along the $\mathbf{z}$-axis can be approximated by [18]:

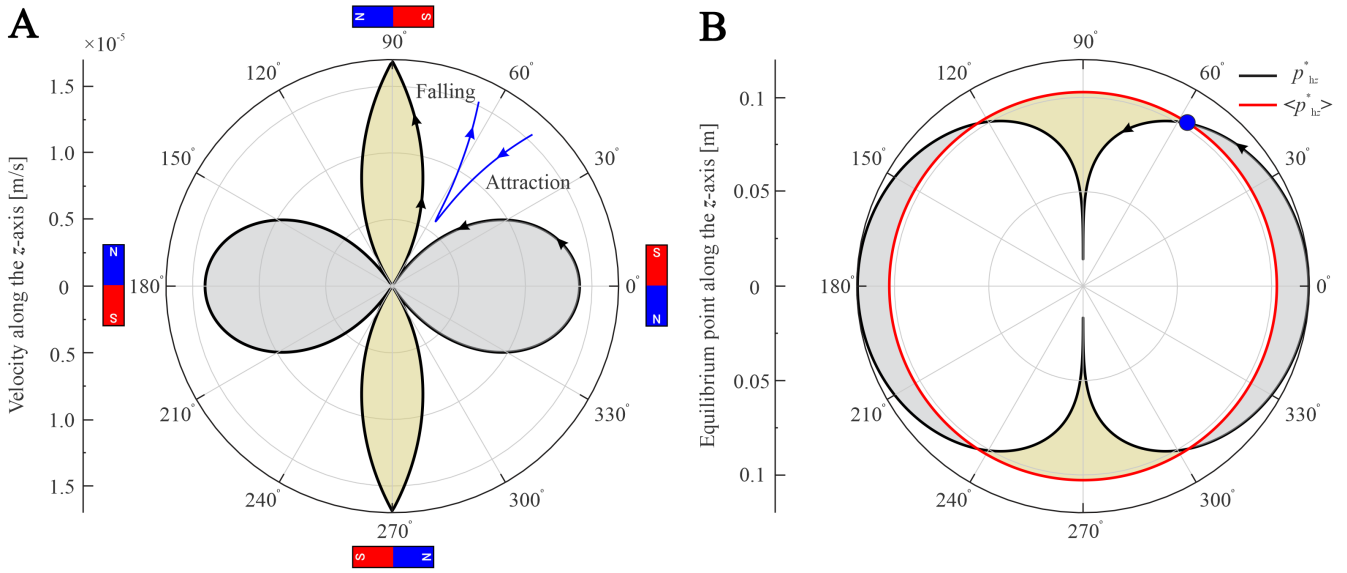

Fig. 5. Rotating of an RPM when swimming with a small AoA and active suspension. (A) The velocity of the UHMD along the **z**-axis, obtained by Equation (6) when the RPM is allowed to rotate in $[0, 2\pi)$, where it gets attracted when the magnetic pulling force is strongest and falls due to gravity when the field gradient pulling decreases. (B) The position of the device (black line) and the equilibrium point of the position (red line) obtained by ${}^{\mathrm{a}}\dot{p}_{\mathrm{h}_z} = 0$, $M = 18.89$ A·m^2, $m_{\mathrm{h}} = 6.23 \times 10^{-4}$ A·m^2, $\rho_{\mathrm{h}} = 7700$ kg·m^{-3}, and $\rho_{\mathrm{f}} = 971$ kg·m^{-3}. The equilibrium point (blue dot) is the same for (A) and (B) [18].

$$ {}^{\mathrm{a}}\dot{p}_{\mathrm{h}_z} = \sum_{i=1}^{2} \frac{\ln\left(\frac{l_i}{a_i}\right) + 0.193}{4\pi\eta} \left(\frac{3\mu_0 M m_{\mathrm{h}}}{2\pi\ {}^{\mathrm{a}}p_{\mathrm{h}_z}^4} - \Delta\rho g V \right), \quad (6) $$

where $\Delta\rho := (\rho_{\mathrm{h}} - \rho_{\mathrm{f}})$, ρ_{h} and ρ_{f} are the density of the UMHD and the fluid, respectively, g is the gravitational acceleration and V is the volume of the UHMD. The viscosity of the fluid is denoted by η and l_1 and a_1 are the length and radius of the filament respectively, where l_2 and a_2 are the length and radius of the head, respectively. Fig. 5(A) shows the velocity of the UHMD along the **z**-axis when the RPM is allowed to rotate with an angle $2\pi k$ for some integer k. The velocity of the UHMD follows a periodic pattern of being attracted most when the RPM is orientated with a single pole towards the device (i.e. for $0°$ and $180°$) where the field gradient pulling is highest. The device will be attracted less, and thus fall due to gravity when the RPM is orientated between these states (i.e. for $90°$ and $270°$), causing the RPM and UHMD to become uncoupled magnetically. When moving along the circle, starting from $0°$, the attraction decreases causing the velocity due to attraction to decrease too, until the equilibrium point is reached at approximately $60°$. Here, gravity is balanced by the magnetic pulling force of the RPM, after which the device starts falling and reaches a maximum velocity when the RPM is orientated at $90°$. The attraction will increase again when moving towards the $180°$, consequently increasing the velocity due to the attraction of the magnetic field.

Fig. 5(B) shows the position of the UHMD along the **z**-axis (black curve) and the equilibrium point of this position (red curve), which is obtained by ${}^{\mathrm{a}}\dot{p}_{\mathrm{h}_z} = 0$. It can be seen that at the intersection of the black and red curve (blue dot), the device is in equilibrium, which can also be seen in Fig. 5(A) at the moments where ${}^{\mathrm{a}}\dot{p}_{\mathrm{h}_z} = 0$. Equation (6) suggests that the equilibrium line for a representative case should be at 0.1 m.

III. EXPERIMENTAL RESULTS

To experimentally determine the input-output boundedness, a setup with an RPM attached to a robotic arm and a UHMD placed in a viscous medium was made to evaluate the different input parameters found in the numerical model. Inputs were also based on the results found in previous experiments [17].

A. Experimental Setup

The UHMD consists of a magnetic head and a helical tail. The head is a cylinder of NdBFe Grade-N52 which is rigidly attached to a helical tail with a fast drying glue. The cylinder axis, which is the direction of the magnetic moment of the head, and the long axis of the tail, which is the direction of the thrust, are perpendicular. The cylinder of 1 mm in diameter by 1 mm in height provides a magnetic moment of $m_{\mathrm{h}} = 6.23 \cdot 10^{-4}$ A·m^2. An aluminium wire of 0.19 mm in diameter is wound into a right-handed helical body of 11.7 mm in length by 0.94 mm in outer diameter. The resulting UHMD is contained inside a $140{\times}50{\times}55$ mm^3 plexiglass container with silicone oil (Carl Roth Gmbh & Co. Kg, Karlsruhe, Germany), with a viscosity of 1 Pa·s and density of 971 kg·m^{-3}, which allows the approach of a Reynolds number (Re) on the order of 10^{-2}. A rotating magnetic field is generated using a cylinder of NdBFe Grade-N45 35 mm in diameter by 20 mm in height with a magnetic moment of $M = 18.89$ A·m^2. This permanent magnet is rotated by using a Maxon 18 V brushless DC motor. The pose of this RPM is

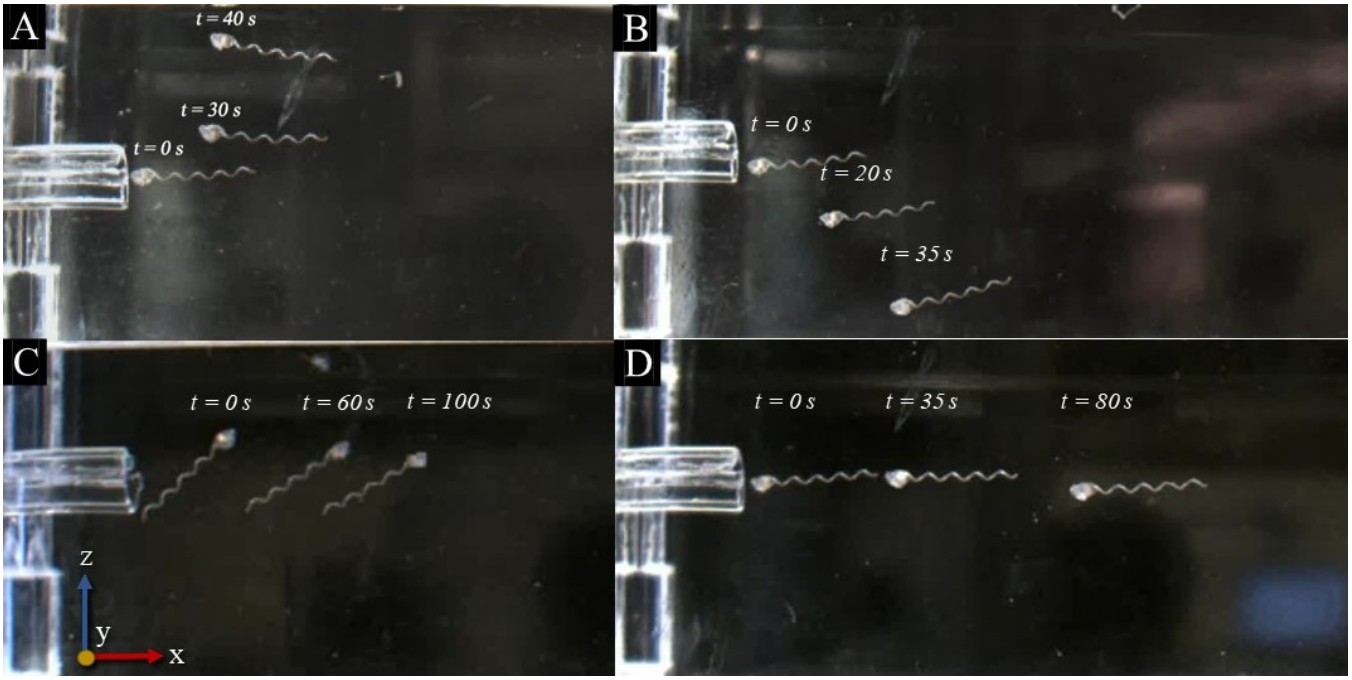

Fig. 6. To make sure the UHMD swims in straight trajectories, self-compensation can be deployed in different ways to counteract the different forces that act on the system. (A) The UHMD is attracted too much by the magnetic pulling force and swims upwards. (B) The UHMD sinks under its own weight due to gravity when there is not enough compensation of the magnetic field. (C) The UHMD directly compensates gravity with the thrust created by rotation. The device has an average AoA of $37.8° \pm 2.9°$. (D) The UHMD is bounded by active suspension where the attraction and gravitational forces are self-compensated. The device has an average AoA of $6.3° \pm 2.2°$.

controlled using a KUKA 6-DOF manipulator (KUKA KR-10 1100-2, KUKA, Augsburg, Germany), as shown in Fig. 1, with RoboDK software (RoboDK Inc., Montreal, Canada). The runs are recorded using two FLIR Blackfly cameras (Teledyne FLIR LLC, Wilsonville, Oregon) aimed at the $\mathbf{x}/\mathbf{z}$- and $\mathbf{x}/\mathbf{y}$-axis Straight runs are initiated (Fig. 6) such that the UHMD swims along a horizontal path, far from any solid boundary and from the silicone-air interface. The same helical device was used to investigate swimming with gravity compensation and active suspension.

B. Input parameters

To determine the optimal input values for the different parameters, a UHMD is actuated by a robotically controlled RPM which moves along the $\mathbf{x}$-axis with a rotation axis $\widehat{\mathbf{\Omega}}_{\mathrm{a}} = [1, 0, 0]^T$ when $\beta = 0°$. A fixed value of 3.5 Hz was chosen for the frequency f_{a}, being below the step-out frequency. To determine the upper and lower bounds of the values for the different parameters of the RPM, the inputs were varied one by one and tested for 10 runs. The velocity of the RPM was tested between $0.4 \leq \mathbf{v}_{\mathrm{a}} \leq 0.8$ mm/s, the distance between the RPM and the device $70 \leq |{}^{\mathrm{a}}\mathbf{p}_{\mathrm{h}}(t_0)| \leq 90$ mm and a pitch angle of $11° \leq \beta_{\mathrm{a}} \leq 13°$. The results can be found in Table I, which shows the different runs with the used inputs and resulting outputs. For every specific case, the gain γ is determined with Equation (5), which results in the average gain of the different trials. It must be noted that due to the limits of the container and the medium, $\gamma < 1$ will be true for every case, but this does not mean that the case was following a straight trajectory along the $\mathbf{x}$-axis. To determine how long each run stayed bounded, it was calculated when $\gamma < 0.02$. Above this value, the run was no longer following a straight trajectory along the $\mathbf{x}$-axis.

During every run, the device drifted along the $\mathbf{y}$-axis, causing it to drift out of reach of the magnetic field caused by the RPM (Fig. 8A). To combat this, the trajectory of the RPM was changed to follow the drift of the device, such that $\mathbf{p}_{\mathrm{a}} = [p_x, p_y, 0]^T$ (Fig. 8B).

C. Experimental results

Fig. 6 shows the different cases with different swimming methods of the UHMD are shown. Without any form of self-compensation, the device either is attracted too much by the magnetic field (Fig. 6(A)) or sinks under its own weight (Fig. 6(B)). It can be noted that for the cases that fell under their own weight, the average gain was $\gamma = 0.29 \pm 0.03$ (Table I: numbers 3, 5, 7). The cases which were attracted more had an average gain of $\gamma = 0.17 \pm 0.01$ (Table I: numbers 4, 6, 8). It can also be shown clearly in the length of bounded parts of the trajectory of these cases, that the average bounded trajectory is very short, indicating too much attraction or too much influence of gravity.

However, when the RPM is positioned under an angle of $41°$, the device has an average AoA of $37.8° \pm 2.9°$ during the 100 s run shown in Fig. 6(C). The average speed of the device is 0.193 mm/s along a trajectory of 19.3 mm, about 1.65 times its body length. The gain of the bounded trajectory is $\gamma = 0.029$.

One true bounded result with active suspension was found at the input parameters $\mathbf{v}_{\mathrm{a}} = 0.68$ mm/s, $|{}^{\mathrm{a}}\mathbf{p}_{\mathrm{h}}(t_0)| =$

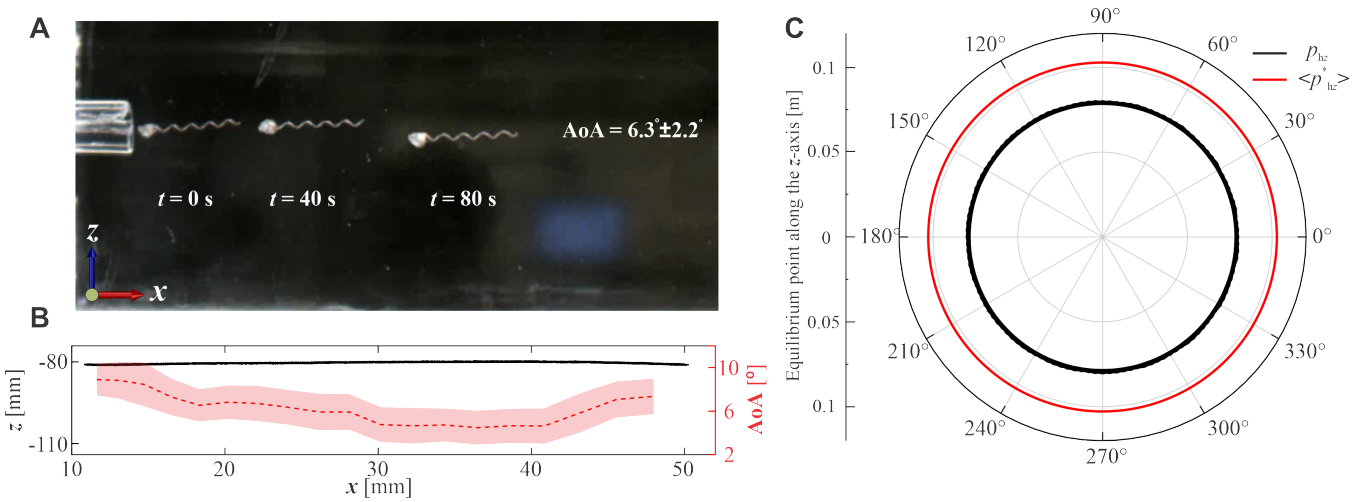

Fig. 7. The bounded case where the UHMD propels itself with a small AoA and with active suspension. (A,B) The trajectory of the UHMD for 80 s along a trajectory of 44.6 mm with an AoA of $6.3° \pm 2.2°$ and a $|^{a}\mathbf{p}_{h}(t_0)| = 80.9$mm. (C) The equilibrium line predicted by Equation (6) at 0.1 m (red circle) and the experimentally determined equilibrium at approximately 0.08 m (black circle).

80.9 mm, $\beta_a = 12°$, $f_a = 3.5$ Hz (One trial from case number 1 in Table 1).

The device moved for 80 s along a path of 44.6 mm, or 3.81 times its body length (Fig. 6(D)). It had an average velocity of 0.308 mm/s and an average AoA of $6.3° \pm 2.2°$. The gain of this case is $\gamma = 0.02$ which shows a bounded output. The device remained bounded until it met the constraints of the container due to the drift.

Drift was encountered in every case. In Fig. 8, an example of drift in a trajectory can be seen with the input parameters of case number 4. In the case shown in Fig. 8A, the travel distance along the $\mathbf{x}$-axis of the device was 19.2 mm over 40 s, swimming with an average speed of 0.48 mm/s. The total drift along this trajectory was 10.6 mm, which means that for every millimeter the device travelled, it drifted 0.55 mm along the $\mathbf{y}$-axis.

It was also found that varying the starting $\mathbf{x}$-position of the RPM $^{a}\mathbf{p}_{h,x}(t_0)$ with respect to the starting point of that of the UHMD, had a great impact on the trajectory of the UHMD. This changes $^{a}\mathbf{p}_{h}$, but also the orientation of the magnetic field with respect to the UHMD. This position was tested for 5 mm $\leq {}^{a}\mathbf{p}_{h,x}(t_0) \leq 25$ mm, where $^{a}\mathbf{p}_{h,x}(t_0) = 25$ mm was used in all cases except for case number 2 (Table I: number 2), where $^{a}\mathbf{p}_{h,x}(t_0) = 5$ mm was used, which resulted in a maximal change of $^{a}\mathbf{p}_{h,x}(t_0) = 0.9$ mm or 0.07 body lengths. It must be noted that the average bounded trajectory of case number 2 is longer ($\mathbf{p}_{h,x} = 14.5$ mm) than that of case number 1 ($\mathbf{p}_{h,x} = 11.2$ mm), where the bounded case was found. However, the longest bounded trajectory was 26.8 mm, after which $\gamma > 0.02$.

D. RFT model and Reduced order model

The values for the input parameters used in the RFT model to create a bounded case differ from the values discovered experimentally. Though the frequency f_a and pitch angle β_a seem similar, more significant differences can be found for the RPM velocity $\mathbf{v}_a$ and the distance between the RPM and the UHMD $|^{a}\mathbf{p}_{h}(t_0)|$. The drift found in the model however could also be found experimentally, where moving the RPM with the trajectory of the UHMD proved to keep the UHMD bounded, but the drift seen experimentally is much larger than predicted by the model.

TABLE I

INPUTS OF THE RPM AND THE RESULTING EXPERIMENTALLY MEASURED OUTPUT

Number	**Inputs**				**Average Gain**	**Length straight trajectory**	**Trials**
nr. [–]	f_a [Hz]	β_a [°]	$\lvert^{a}\mathbf{p}_{h}(t_0)\rvert$ [mm]	$\mathbf{v}_a$ [mm/s]	γ [–]	$\mathbf{p}_{h,x}$ [mm]	**n** [–]
1	3.5	12	80.9	0.68	0.24 ± 0.088	11.0 ± 12.1	10
2	3.5	12	80	0.68	0.29 ± 0.05	13.7 ± 8.88	13
3	3.5	11	80.9	0.68	0.31 ± 0.014	3.95 ± 0.97	10
4	3.5	13	80.9	0.68	0.18 ± 0.015	1.97 ± 1.79	10
5	3.5	12	90.8	0.68	0.26 ± 0.005	2.10 ± 0.20	10
6	3.5	12	71	0.68	0.16 ± 0.005	0.70 ± 0.47	10
7	3.5	12	80.9	0.40	0.31 ± 0.009	5.81 ± 0.91	10
8	3.5	12	80.9	0.80	0.17 ± 0.015	2.89 ± 1.38	10

The measured output y $(\min({}^{a}\mathbf{p}_{h_z}(t)) - \max({}^{a}\mathbf{p}_{h_z}(t)))$, resulting in gain γ calculated with Equation (5) with which the length of the straight parts of the trajectories $\mathbf{p}_{h,x}$ were determined. The inputs are frequency f_a, pitch angle β_a, initial distance between UHMD and RPM $|^{a}\mathbf{p}_{h}(t_0)|$ and velocity of the RPM $\mathbf{v}_a$. The number of trials is $\mathbf{n}$

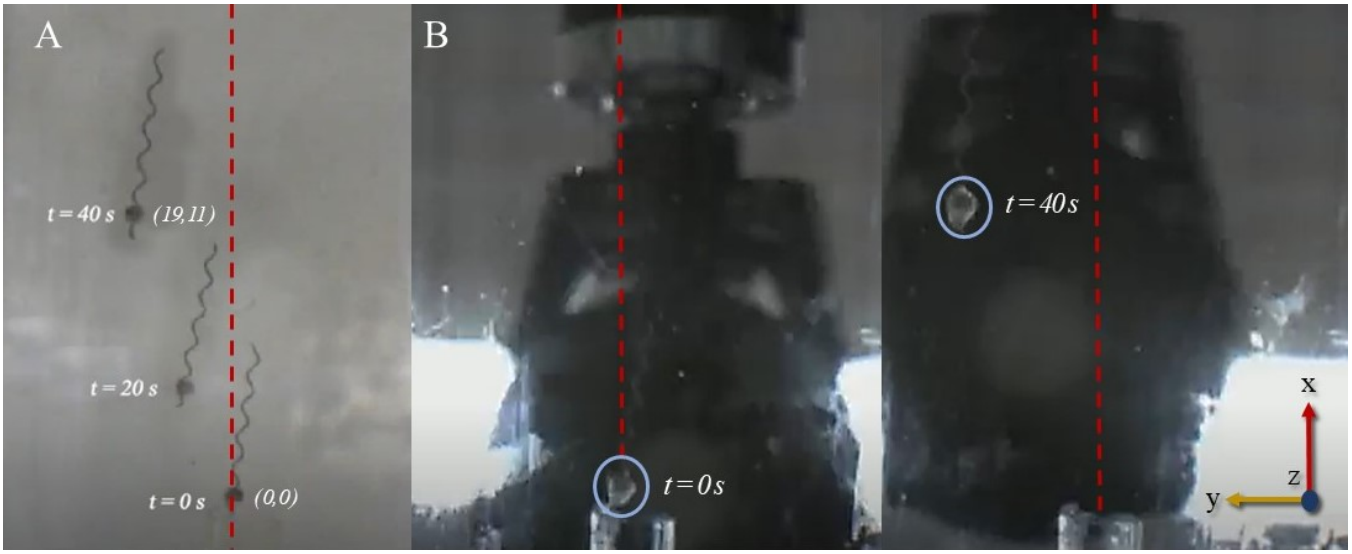

Fig. 8. A drift along the $\mathbf{y}$-axis can be seen in the trajectory of the UHMD for all different cases. The red line shows the $\mathbf{x}$-axis and the trajectory that the UHMD would follow without drift. (A) The device drifts 0.55 mm in $\mathbf{y}$-direction for every millimeter travelled forward. (B) The path of the RPM is changed to move along with the drift.

The reduced order model from Equation (6) predicts that the equilibrium point of the bounded case should be at ${}^{\mathrm{a}}\mathbf{p}_{\mathrm{h},z} = 0.1$ m. The experiments showed however that this was at approximately 0.08 m (Fig. 5(C)). The differences between the models and the experiments can be attributed to deviations in certain parameters (magnetic moments of the RPM and the UHMD, geometric properties of the UHMD and inhomogeneities in the fluid) that change the output of the system. Even though the differences between the predicted input parameters and the experimental results are significant, it can still be claimed that both models represent different parts of the dynamics of a UHMD actuated by an RPM. The trajectories and orientation of the UHMD are well represented and can be used to predict the behaviour when tested *in vitro*.

E. Drifting of the device

The drift of the device showed to be a limitation when controlling the device. Since it drifted out of reach of the RPM, it could no longer be controlled if the RPM didn't move along with the trajectory of the device. Drift will also prove to be a problem when navigating the device through heterogeneous environments or larger volumes.

Drift for these small devices can be caused by wall effects where the drag on the device increases when the distance to a boundary decreases [19]. In this case, the device is not close enough to any boundaries for these forces to play a significant role in the drag on the device.

The device also showed a wobbling motion in which the device moved slightly up and down along the long axis of the body, as is also explained by Equation (6) and in Fig. 5. More wobbling of the device occurs due to lower actuation frequencies, where the uncoupling of the RPM and the UHMD, and then the attraction, can be seen more clearly. Here, the drift velocity becomes higher and the forward velocity relatively lower due to interaction between the device and the surrounding medium [20], [16]. Determining the frequency spectrum and therefore the step-out frequency of the device could reduce the wobbling motion and thus improve the trajectory of the device.

To sustain a pure translation along the $\mathbf{x}$-axis, in the force and torque equilibria acquired by RFT, there is no resulting force perpendicular to the long axis of the UHMD. However, the torque required to achieve this translation includes a torque along and perpendicular to the $\mathbf{x}$-axis, which can be regarded as an actuation and stabilizing torque [20]. This stabilizing torque can be achieved by using more than one actuator, like other magnets [21] or acoustic levitation [19]. This, however, will obstruct the dexterity of the actuator, possibly making it harder to use when applied to manipulate the UHMD in hard-to-reach places in the human body.

Another factor which can attribute to the drift is the placement of the magnetic head with respect to the helical tail. If this magnet is placed further away from the center line, the magnetic forces on the head will also be off-center [20].

F. Robustness of the system

The experimental results show one real case of boundedness. However, with the exact same inputs, 10 other runs were also tested, none of which were bounded for a longer period of time. For the other cases, there were only small changes in for example pitch angle β_{a} or starting position $|{}^{\mathrm{a}}\mathbf{p}_{\mathrm{h}}(t_0)|$, as can be seen in the results of case 1 and 2 in Table I, with none of them resulting in a bounded case. This shows how non-robust the system is; the slightest changes give different results, even when the inputs of the actuator remain the same and the environment is as controlled as possible. However, it must also be noted that due to the open-loop control of the experiments and the environment where the device is deployed, it can not

be expected that the system is as robust when compared to closed-loop control. The naturally occurring forces acting on the device and inhomogeneities in the medium and of the device causing changes in the orientation of the device can not be compensated in real-time by adjusting the input parameters of the RPM.

IV. DISCUSSIONS

The UHMD used has a length of 11.7 mm with a magnetic head of 1 mm $\times$ 1 mm. For testing the theory of active suspension with near zero AoA, the size is not that relevant, as long as it is on the low end of macroscale. To assure the correct operation of the UHMD *in vivo*, the size of the devices should be reduced so no damage can be done to surrounding tissue. For future work in investigating active suspension, smaller UHMDs on microscale should be used to test the different fluidic and external forces and torques on the device and investigate the robustness of the system. When manufacturing these microrobots, it has to be taken into account that the magnetic head is centred properly and that chances for inhomogeneities in the head and body should be reduced as much as possible.

The drift mentioned in the previous section 'EXPERIMENTAL RESULTS' might obstruct the control of the device in larger volumes. However, when deploying the UHMD in a lumen, wall effects play a role in the propulsion of the device. Yang et al. have found that these wall effects could contribute to the control of the device [22]. It will have to be investigated which effects these forces have on a similar helical magnetic device used in this paper and how the device acts in environments with a laminar flow present.

V. CONCLUSIONS

This work showed which physical boundaries are needed to achieve a bounded run with a small AoA with a UHMD. A small AoA can be desirable when moving through lumen-like environments or environments with heterogeneous structural properties. To control this AoA, an open-loop system can be desirable when the orientation of the device can not be accurately determined due to the low resolution of some imaging techniques. The propulsion of a UHMD with a small AoA controlled by an open-loop system was investigated. A numerical model based on resistive force theory and a reduced order model were used to predict the input values of the actuator (rotational frequency, distance between the RPM and UHMD, translational velocity and pitch angle), which were then tested experimentally. In the experiments, it was shown it is possible to create a bounded response of the UHMD by either gravity compensation or active suspension. Active suspension was achieved by swimming with an AoA of $6.3^\circ \pm 2.2^\circ$. This has shown that the RFT model and reduced order model can be used to predict the dynamic behaviour of the UHMD. Factors like wobbling and drift cause instability in the system, but there are ways to overcome this; by manufacturing the device in ways that inhomogeneities are reduced and nearing the step-out frequency of the system. This work shows how propulsion with a small angle of attack using active suspension is possible, which is suitable for lumen-like and heterogeneous environments.

VI. ACKNOWLEDGEMENTS

I would like to thank R.J. Struik, Department of Biomechanical Engineering, University of Twente, for the assistance in the lab, the experiments would've never been completed without him, L.J.W. Ligtenberg, Department of Biomechanical Engineering, University of Twente, for his insights of the subject and his helpfulness and lastly I.S.M. Khalil, Department of Biomechanical Engineering, University of Twente, for the guidance of this project, his enthousiasm and showing me more of what the field of microrobots has to offer.

REFERENCES

[1] T. W. R. Fountain, P. V. Kailat, and J. J. Abbott. "Wireless control of magnetic helical microrobots using a rotating-permanent-magnet manipulator," in *Proc. IEEE Int. Conf. Robot. Autom.*, 2011, pp. 576–581.

[2] B. J. Nelson, I. K. Kaliakatsos, J. J. Abbott."Microrobots for minimally invasive medicine." Annual review of biomedical engineering vol. 12: 55-85, 2010

[3] M. Li, X. Hu, Y. Zhao, N. Jiao, "An Overview of Recent Progress in Micro/Nanorobots for Biomedical Applications." Adv. Mater. Technol. 2023

[4] C. K. Schmidt, M. Medina-Sánchez, R. J. Edmondson, and O. G. Schmidt. "Engineering microrobots for targeted cancer therapies from a medical perspective." Nature communications, 11(1), 5618., 2020

[5] I. S. M. Khalil, A. Adel, D. Mahdy, M. M. Micheal, M. Mansour, N. Hamdi and S. Misra. "Magnetic localization and control of helical robots for clearing superficial blood clots." APL Bioeng. 2019;3(2):026104. Published 2019 May 20.

[6] H. Zhang, D. W. Hutmacher, F. Chollet, A. N. Poo and E. Burdet. "Microrobotics and MEMS-Based Fabrication Techniques for Scaffold-Based Tissue Engineering." Macromolecular Bioscience, 5(6), 477-489.2005

[7] L. Hines, K. Petersen, G. Z. Lum and M. Sitti. "Soft Actuators for Small-Scale Robotics." Advanced Materials, 29(13), 1603483, 2017

[8] J. J. Abbott, K. E. Peyer, M. C. Lagomarsino, L. Zhang, L. Dong, I. K. Kaliakatsos, and B. J. Nelson, "How should microrobots swim?," *Int. J. Robot. Res.* vol. 28, no. 11–12, pp. 1434–47, 2009.

[9] A. W. Mahoney, J. C. Sarrazin, E. Bamberg, and J. J. Abbott, "Velocity control with gravity compensation for magnetic helical microswimmers," *Adv. Robot.*, vol. 25, no. 8, pp. 1007–1028, 2011.

[10] B. J. Nelson and K. E. Peyer, "Micro- and Nanorobots Swimming in Heterogeneous Liquids," ACS Nano, vol. 8, no. 9, pp. 8718–8724, Sep. 2014

[11] N. D. Nelson, J. Delacenserie and J. J. Abbott, "An empirical study of the role of magnetic, geometric, and tissue properties on the turning radius of magnetically driven screws," 2013 IEEE International Conference on Robotics and Automation, pp. 5372-5377, 2013

[12] R. Venezian and I. S. M. Khalil, "Understanding robustness of magnetically driven helical propulsion in viscous fluids using sensitivity analysis," *Adv. Theory Simul.*, vol. 5, no. 4, pp. 2100519, 2022.

[13] T. Xu, G. Hwang, N. Andreff, and S. Régnier, "Planar path following of 3-D steering scaled-up helical microswimmers," *IEEE Trans. Robot.*, vol. 31, no. 1, pp. 117-127, 2015.

[14] S. Pane, G. Faoro, E. Sinibaldi, V. Iacovacci, and A. Menciassi, "Ultrasound acoustic phase analysis enables robotic visual-servoing of magnetic microrobots," *IEEE Trans. Robot.*, vol. 38, no. 3, pp. 1571-1582, 2022.

[15] C. Li, S. Misra, and I. S. M. Khalil, "Closed-Loop control characterization of untethered small-scale helical device in physiological fluid with dynamic flow rates," *Adv. Intell. Syst.*, 2200322, 2023.

[16] B. Wang, Y. Zhang, and L. Zhang, "Recent progress on micro- and nano-robots: towards in vivo tracking and localization," Quant. Imaging Med. Surgery; Vol 8, No 5 (June 30, 2018) Quant. Imaging Med. Surg., 2018.

[17] L. J. W. Ligtenberg and I. S. M. Khalil. “Input-Output boundedness of a magnetically-actuated helical device,” in *Proc. IEEE Int. Conf. Robot. Autom*, 2023.

[18] L. J. W. Ligtenberg, I. A. A. Ekkelkamp, F. Halfwerk, C. Goulas, J. Arens, M. Warle, I. S. M. Khalil. “Helical Propulsion in Low-Re Numbers with Near-Zero Angle of Attack,” accepted for *IEEE:IROS*, 2023

[19] L. Xu, D. Gong, K. Chen, J. Cai and W. Zhang; “Acoustic levitation applied for reducing undesired lateral drift of magnetic helical microrobots.” Journal of Applied Physics 14 November 2020; 128 (18): 184703, 2020.

[20] K. Peyer, L. Zhang, B. Kratochvil and B. Nelson. “Non-ideal Swimming of Artificial Bacterial Flagella Near a Surface.” Proceedings - IEEE International Conference on Robotics and Automation. 96 - 101, 2010

[21] A. Hosney, A. Klingner, S. Misra and I. S. M. Khalil, “Propulsion and steering of helical magnetic microrobots using two synchronized rotating dipole fields in three-dimensional space,” 2015 IEEE/RSJ International Conference on Intelligent Robots and Systems (IROS), Hamburg, Germany, 2015

[22] L. Yang, T. Zhang, H. Huang, H. Ren, W. Shang and Y. Shen, “An On-Wall-Rotating Strategy for Effective Upstream Motion of Untethered Millirobot: Principle, Design, and Demonstration,” in IEEE Transactions on Robotics, vol. 39, no. 3, pp. 2419-2428, June 2023